Inorg. Chem. **2007**, *46*, 7861–7869

^{31}P Magic Angle Spinning NMR Spectroscopy for Probing Local Environments in Paramagnetic Europium-Substituted Wells–Dawson Polyoxotungstates

Wenlin Huang,[†] Lynn C. Francesconi,*[,‡] and Tatyana Polenova*[,†]

Department of Chemistry and Biochemistry, University of Delaware, Newark, Delaware 19716, and Department of Chemistry, City University of New York–Hunter College, 695 Park Avenue, New York, New York 10021

Received March 17, 2007

A series of europium-substituted Wells–Dawson polyoxotungstates were addressed by ^{31}P magic angle spinning (MAS) NMR spectroscopy. The electron–nuclear dipolar interaction dominates the ^{31}P spinning-sideband envelopes. The experimental electron–nuclear dipolar anisotropies were found to be in good agreement with those calculated based on the known crystallographic coordinates and effective magnetic moments and assuming a point-dipole approximation. These electron–nuclear dipolar anisotropies directly report on the anion stoichiometry and on the positional isomerism, indicating that ^{31}P MAS NMR spectroscopy may be a useful and quick analytical probe of the local environment in Wells–Dawson solids containing localized europium paramagnetic centers.

Introduction

Lanthanide-substituted polyoxometalates were first reported by Peacock and Weakley in 1971.[1] Lanthanide ions may exist in multiple oxidation states and coordination numbers, and their incorporation into the oxoanion core leads to functionalized structures with tunable catalytic, photochemical, magnetic, and electronic properties. Therefore, interest in designing lanthanide-containing polyoxoanionic compounds for novel applications has been steadily growing in the past decade.

In parallel, actinide derivatives of polyoxoanionic compounds are drawing increased attention because of the potential opportunities for efficient separation of actinides by sequestration and reduction in a Wells–Dawson matrix.[2–4] The design of efficient actinide protocols to separate actinides from lanthanides as well as neighboring actinides has posed significant challenges to date[5–9] and is of great importance in the areas of radioactive waste management, bioremediation, and development of radiotherapeutic agents. The α_2-$P_2W_{17}O_{61}^{10-}$ species has been successful in solvent extraction techniques for the separation of radiolanthanides from actinides and, in some cases, from each other.[5–21]

* To whom the correspondence should be addressed. E-mail: lfrances@hunter.cuny.edu (L.C.F.), tpolenov@chem.udel.edu (T.P.). Tel.: (212) 772-5353 (L.C.F.), (302) 831-1968 (T.P.). Fax: (212) 772-5332 (L.C.F.), (302) 831-6335 (T.P.).

† University of Delaware.

‡ City University of New York

(1) Peacock, R. D.; Weakley, T. J. R. *J. Chem. Soc. A* **1971**, 1836.
(2) Antonio, M. R.; Soderholm, L.; Jennings, G.; Francesconi, L. C.; Dankova, M.; Bartis, J. *J. Alloys Compd.* **1998**, *277*, 827–830.
(3) Chiang, M.-H.; Soderholm, L.; Antonio, M. R. *Eur. J. Inorg. Chem.* **2003**, *2003*, 2929–2936.
(4) Chiang, M.-H.; Williams, C. W.; Soderholm, L.; Antonio, M. R. *Eur. J. Inorg. Chem.* **2003**, *2003*, 2663–2669.
(5) Choppin, G. *Radiochim. Acta* **2004**, *92*, 519–523.
(6) Choppin, G. R. *J. Nucl. Radiochem. Sci.* **2005**, *6*, 1–5.
(7) Musikas, C. *NATO Science Series, Series 2: Environmental Security*; Kluwer Academic Publishers: Dordrecht, The Netherlands, 1999; Vol. 53, pp 99–122.
(8) Nash, K. L. In *Proceedings of Actinide Conference 2005*; May, I., Alvarez, R., Bryan, N., Eds.; Royal Society of Chemistry: Cambridge, U.K., 2006; Vol. 8, pp 465–472.
(9) Roberto, J.; Diaz de la Rubia, T. *Basic Research for Advanced Nuclear Energy Systems*; Office of Science U.S. Department of Energy: Washington, DC, 2006.
(10) Bion, L.; Moisy, P.; Madic, C. *Radiochim. Acta* **1995**, *69*, 251–257.
(11) Chartier, D.; Donnet, L.; Adnet, J. M. *Radiochim. Acta* **1998**, *83*, 129–134.
(12) Haraguchi, N.; Okaue, Y.; Isobe, T.; Matsuda, Y. *Inorg. Chem.* **1994**, *33*, 1015–1020.
(13) Kamoshida, M.; Fukasawa, T.; Kawamura, F. *J. Nucl. Sci. Technol.* **1998**, *35*, 185–189.
(14) Malikov, D. A.; Milyukova, M. S.; Kuzovkina, E. V.; Myasoedov, B. F. *Sov. Radiochem. Engl. Transl.* **1993**, *35*, 465–471.
(15) Malikov, D. A.; Milyukova, M. S.; Myasoedov, B. F. *Sov. Radiochem. Engl. Transl.* **1989**, *31*, 425–430.
(16) Milyukova, M. S.; Varezhkina, N. S.; Myasoedov, B. F. *J. Radioanal. Nucl. Chem.* **1986**, *105*, 249–256.
(17) Milyukova, M. S.; Varezhkina, N. S.; Myasoedov, B. F. *J. Radioanal. Nucl. Chem.* **1988**, *121*, 403–408.
(18) Milyukova, M. S.; Varezhkina, N. S.; Myasoedov, B. F. *Sov. Radiochem. Engl. Transl.* **1990**, *32*, 361–367.

10.1021/ic700521p CCC: $37.00
Published on Web 08/23/2007

The α_1-$P_2W_{17}O_{61}^{10-}$ isomer shows more selectivity in complexing to Ln^{III} ions and may prove to be a better complexant to separate radiolanthanides from each other and lanthanides from actinides. For the production of high-specific-activity radiolanthanides that are required for the development of radiopharmaceuticals, there is also a need to separate neighboring radiolanthanides. The methods that are used presently include solvent extraction and ion-exchange chromatography, both using phosphonate ligands. However, faster, more efficient methods are sought for the separation of tracer quantities of radiolanthanides for therapy. Polyoxometalates, specifically the α_1-$P_2W_{17}O_{61}^{10-}$ isomer, may be particularly useful in this effort. Establishing robust separation methods requires a fundamental understanding of the chemistry of lanthanide and actinide derivatives of polyoxoanionic compounds, including detailed knowledge of their redox properties, positional isomerism, as well as anion stoichiometry in the solid state.

To address these aspects of polyoxometalate structure and reactivity, appropriate site-specific probes are required. Many of the actinide derivatives of polyoxoanions are paramagnetic and can therefore be employed as intrinsic markers of the local geometry and electronic environment (i.e., the effective magnetic moment, in turn, reflecting the oxidation state of the actinide in the anion) in solid-state NMR experiments detecting a nucleus dipolar coupled to the electron(s) of the paramagnetic site. We initiated work in this area by investigating a series of nonradioactive paramagnetic europium-substituted Keggin solids, which serve as models of radioactive actinide-substituted polyoxometalates. In our recent report, we have demonstrated that paramagnetism of Eu^{III} centers can be employed as a site-specific probe of the local geometry of these systems.[22] As anticipated, ^{31}P solid-state magic angle spinning (MAS) NMR spectra in these compounds are dominated by the anisotropic dipolar interaction between the nuclear (^{31}P) and the electronic magnetic moments, giving rise to broad asymmetric spinning-sideband envelopes. These envelopes are very sensitive to the local geometry of the paramagnetic centers. Geometric information can be readily extracted by numerical simulations of the spectra. Nuclear probes other than ^{31}P (e.g., ^{13}C, ^{1}H, ^{2}H, ^{6}Li, and ^{7}Li) have also been previously used to gain information on the local structure in various inorganic solids.[23−31]

In this study, we addressed a series of paramagnetic europium-substituted Wells−Dawson solids, by ^{31}P MAS NMR spectroscopy. We examined the paramagnetic electron−nuclear dipolar interaction in the Wells−Dawson compounds prepared as different positional isomers (α_1 and α_2 derivatives) and for each isomer as a function of the anion stoichiometry and local packing (monomeric 1:1 and dimeric 1:2 species). Our results indicate that the electron−nuclear dipolar tensor is a sensitive reporter of the local geometry of the paramagnetic centers in the Wells−Dawson solids, allowing for the different positional isomers and different anion stoichiometries to be readily inferred from the spectral line-shape simulations. ^{31}P solid-state NMR spectroscopy thus provides a sensitive probe of local environments in these europium-substituted Wells−Dawson polyoxoanionic solids.

Experimental Section

Materials and Syntheses. All chemicals were obtained from Aldrich or Fisher and used without further purification. Sodium tungstate dihydrate ($Na_2WO_4 \cdot 2H_2O$), sodium metavanadate ($NaVO_3$), tetrabutylammonium bromide [$(n\text{-}C_4H_9)_4NBr$], cesium chloride (CsCl), and vanadyl sulfate ($VOSO_4$) were purchased from Aldrich Chemicals. Hydrochloric acid, glacial acetic acid, phosphoric acid (85%), sulfuric acid, and bromine were purchased from Fisher Scientific.

The vanadium-substituted Wells−Dawson complexes include 1-$K_7P_2VW_{17}O_{62} \cdot 18H_2O$ (α_2 isomer, **I**), 4-$K_7P_2VW_{17}O_{62} \cdot 17H_2O$ (α_1 isomer, **II**), and 1,2-$K_8P_2V_2W_{16}O_{62} \cdot 18H_2O$ (**III**). These compounds were synthesized following the procedure reported by Abbessi and co-workers.[32]

The europium-substituted Wells−Dawson complexes include two α_2 isomers, the monomeric $Al_2(H_3O)_8[Eu(H_2O)_3(\alpha_2\text{-}P_2W_{17}O_{61})]_2 \cdot 29H_2O$ (**IV**) and the dimeric $K_{16}(H_3O)[Eu(\alpha_2\text{-}P_2W_{17}O_{61})_2] \cdot 42.5H_2O$ (**V**), as well as two α_1 compounds, the monomeric $K_7[Eu(H_2O)_4(\alpha_1\text{-}P_2W_{17}O_{61})]$ (**VI**) and the dimeric $K_{14}(H_3O)_3[Eu(\alpha_1\text{-}P_2W_{17}O_{61})_2] \cdot 4KCl \cdot 64H_2O$ (**VII**). The synthesis of these compounds and the X-ray crystal structures for **IV**, **V**, and **VII** have been reported recently.[33−39] The schematic representations of the individual anions are shown in Figure 1.

(19) Molochnikova, N. P.; Frenkel, V. Y.; Myasoedov, B. F. *Sov. Radiochem. Engl. Transl.* **1989**, *31*, 322−326.
(20) Termes, S. C.; Pope, M. T. *Transition Met. Chem.* **1978**, *3*, 103−108.
(21) Varezhkina, N. S.; Milyukova, M. S.; Myasoedov, B. F. *J. Radioanal. Nucl. Chem.* **1989**, *135*, 67−76.
(22) Huang, W.; Schopfer, M.; Zhang, C.; Howell, R. C.; Gee, B. A.; Francesconi, L. C.; Polenova, T. *J. Phys. Chem. B* **2006**, *110*, 12340−12350.
(23) Lee, Y. J.; Grey, C. P. *J. Phys. Chem. B* **2002**, *106*, 3576−3582.
(24) Nayeem, A.; Yesinowski, J. P. *J. Chem. Phys.* **1988**, *89*, 4600−4608.
(25) Lee, H.; Polenova, T.; Beer, R. H.; McDermott, A. E. *J. Am. Chem. Soc.* **1999**, *121*, 6884−6894.
(26) Liu, K.; Ryan, D.; Nakanishi, K.; Mcdermott, A. *J. Am. Chem. Soc.* **1995**, *117*, 6897−6906.
(27) Brough, A. R.; Grey, C. P.; Dobson, C. M. *J. Am. Chem. Soc.* **1993**, *115*, 7318−7327.
(28) Tucker, M. C.; Doeff, M. M.; Richardson, T. J.; Finones, R.; Reimer, J. A.; Cairns, E. J. *Electrochem. Solid-State Lett.* **2002**, *5*, A95−A98.
(29) Woehler, S. E.; Wittebort, R. J.; Oh, S. M.; Hendrickson, D. N.; Inniss, D.; Strouse, C. E. *J. Am. Chem. Soc.* **1986**, *108*, 2938−2946.
(30) Brough, A. R.; Grey, C. P.; Dobson, C. M. *J. Chem. Soc., Chem. Commun.* **1992**, 742−743.
(31) Lin, T. H.; Dinatale, J. A.; Vold, R. R. *J. Am. Chem. Soc.* **1994**, *116*, 2133−2134.
(32) Abbessi, M.; Contant, R.; Thouvenot, R.; Herve, G. *Inorg. Chem.* **1991**, *30*, 1695−1702.
(33) Bartis, J.; Dankova, M.; Lessmann, J. J.; Luo, Q.-H.; Horrocks, W. D., Jr.; Francesconi, L. C. *Inorg. Chem.* **1999**, *38*, 1042−1053.
(34) Luo, Q.; Howell, R. C.; Dankova, M.; Bartis, J.; Williams, C. W.; Horrocks, W. D., Jr.; Young, J. V. G.; Rheingold, A. L.; Francesconi, L. C.; Antonio, M. R. *Inorg. Chem.* **2001**, *40*, 1894−1901.
(35) Zhang, C.; Bensaid, L.; McGregor, D.; Fang, X.; Howell, R. C.; Burton-Pye, B.; Luo, Q.; Todaro, L.; Francesconi, L. C. *J. Cluster Sci.* **2006**, *17*, 389−426.
(36) Zhang, C.; Howell, R. C.; Luo, Q. H.; Fieselmann, H. L.; Todaro, L. J.; Francesconi, L. C. *Inorg. Chem.* **2005**, *44*, 3569−3578.
(37) Zhang, C.; Howell, R. C.; McGregor, D.; Bensaid, L.; Rahyab, S.; Nayshtut, M.; Lekperic, S.; Francesconi, L. C. *C. R. Chim.* **2005**, 235−243.
(38) Zhang, C.; Howell, R. C.; Scotland, K. B.; Perez, F. G.; Todaro, L.; Francesconi, L. C. *Inorg. Chem.* **2004**, *43*, 7691−7701.
(39) Zhang, X.; Wang, D.; Dou, J.; Yan, S.; Yao, X.; Jiang, J. *Inorg. Chem.* **2006**, *45*, 10629−10635.

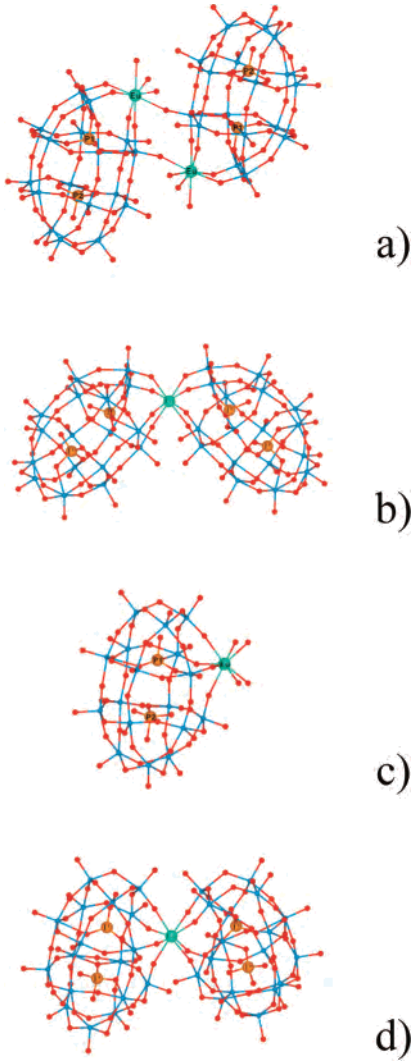

Figure 1. Schematic representations of europium-substituted polyoxotungstate anions: (a) monomeric $Al_2(H_3O)_8[Eu(H_2O)_3(\alpha_2\text{-}P_2W_{17}O_{61})]_2 \cdot 29H_2O$; (b) dimeric $K_{17}[Eu(\alpha_2\text{-}P_2W_{17}O_{61})_2]$; (c) monomeric $K_7[Eu(H_2O)_4(\alpha_1\text{-}P_2W_{17}O_{61})]$; (d) dimeric $K_{14}(H_3O)_3[Eu(\alpha_1\text{-}P_2W_{17}O_{61})_2] \cdot 4KCl \cdot 64H_2O$. The molecules are depicted in a ball-and-stick representation. In the anion, the tungsten atoms are shown in blue and the central P atoms are shown in orange. The europium atoms are shown in green.

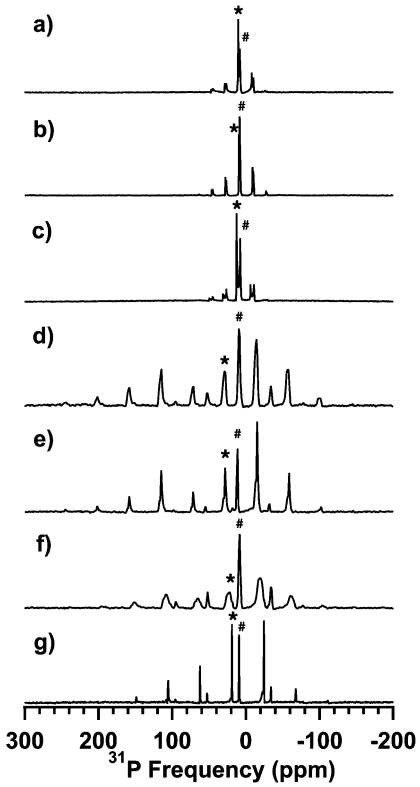

Figure 2. ^{31}P MAS NMR spectra of vanadium-substituted Wells−Dawson compounds (a) 1-$K_7P_2VW_{17}O_{62} \cdot 18H_2O$ (**I**) (α_2 isomer), (b) 4-$K_7P_2VW_{17}O_{62} \cdot 17H_2O$ (**II**) (α_1 isomer), and (c) 1,2-$K_8P_2V_2W_{16}O_{62} \cdot 18H_2O$ (**III**) acquired at the MAS frequency of 3 kHz and of europium-substituted Keggin compounds (d) $Al_2(H_3O)_8[Eu(H_2O)_3(\alpha_2\text{-}P_2W_{17}O_{61})]_2 \cdot 29H_2O$ (**IV**), (e) $K_{17}[Eu(\alpha_2\text{-}P_2W_{17}O_{61})_2]$ (**V**), (f) $K_7[Eu(H_2O)_4(\alpha_1\text{-}P_2W_{17}O_{61})]$ (**VI**), and (g) $K_{14}(H_3O)_3[Eu(\alpha_1\text{-}P_2W_{17}O_{61})_2] \cdot 4KCl \cdot 64H_2O$ (**VII**) acquired at the MAS frequency of 10 kHz. The isotropic bands are marked with asterisks (P1) and pounds (P2). The isotropic chemical shifts are compiled in Table 1 (referenced to 85% H_3PO_4).

Solid-State NMR Spectroscopy. ^{31}P solid-state NMR spectra were acquired at 162.036 MHz (9.4 T) on a Tecmag Discovery spectrometer using a 4 mm Varian T3 probe. A total of 30−40 mg of the sample was packed into zirconium oxide rotors for data collection. The magic angle was adjusted using $NaNO_3$ (by detecting the ^{23}Na MAS NMR signal). ^{31}P NMR spectra were collected at several different spinning frequencies ranging from 1 to 17 kHz. A single 4.3 μs pulse ($\gamma H_1/2\pi = 58.1$ kHz) was employed; the pulse delays of 10 and 60 s were used for europium and vanadium compounds, respectively. The MAS frequency was controlled to within ±2 Hz. A total of 1024 complex data points were acquired. The data were processed by Fourier transformation and baseline correction using the MestRe-C23 NMR data processing software.[40] Isotropic chemical shifts are reported with respect to the 85% H_3PO_4 used as an external reference. ^{31}P spin−lattice relaxation times (T_1) were measured using an inversion−recovery sequence with a recycle delay of 60 s; 64 increments were added up for each free induction decay. ^{31}P spin−spin relaxation times (T_2) were measured using the Carr−Purcell−Meiboom−Gill (CPMG) sequence, at an MAS frequency of 10 kHz, with a rotor-synchronized echo time $\tau = 0.1$ ms, a recycle delay of 60 s, and 64 scans.

Simulations of the NMR Spectra. Numerical simulations of the experimental ^{31}P solid-state NMR spectra were performed on a 1.1 GHz Pentium-4 PC under the Linux environment using the SIMPSON software package.[41] Chemical shielding anisotropy (CSA) tensor components were extracted by numerical simulations of the experimental spectra using the Herzfeld−Berger algorithm[42] implemented in the HBA 1.4.4 program.[43]

Calculation of Electron−Nuclear Dipolar Coupling Tensors. The dipolar coupling tensors between the phosphorus nucleus and the paramagnetic centers in **II**−**VI** and **VIII**−**X** were calculated as described in our recent report,[22] using a home-written program in Mathematica 5.0 (Wolfram, Inc.). The experimental crystallographic coordinates and effective magnetic moments were utilized. For the sake of clarity, here we present a brief summary of the salient points considered in the calculations.

The Hamiltonian for a spin $^1/_2$ nucleus in a paramagnetic system is

(40) Cobas, J.; Cruces, J.; Sardina, F. J. Departmento de Quimica Organica, Facultat de Quimica, Universidad de Santiago de Compostela, Spain, 2000.

(41) Bak, M.; Rasmussen, J. T.; Nielsen, N. C. *J. Magn. Reson.* **2000**, *147*, 296−330.
(42) Herzfeld, J.; Berger, A. E. *J. Chem. Phys.* **1980**, *73*, 6021−6030.
(43) Eichele, K.; Wasylishen, R. E. HBA program, 1.4.4 ed.; 2001.

$$\hat{H} = \hat{H}_{\text{Zeeman}} + \hat{H}_{\text{RF}} + \hat{H}_{\text{FC}} + \hat{H}_{\text{DIP}}^{\text{paramagn}} + \hat{H}_{\text{CSA}} \quad (1)$$

The terms in the Hamiltonian represent the Zeeman, the radio-frequency field, the Fermi contact shift, the electron−nuclear dipolar interaction, and the chemical shift anisotropy.

The Fermi contact interaction in paramagnetic systems gives rise to isotropic shifts of the resonance lines and is expressed as

$$\hat{H}_{\text{FC}} = \vec{I}(A_{\text{d}} + A_{\text{p}})\vec{S} \quad (2)$$

where A_{d} is the hyperfine coupling constant, which is related to a direct delocalization mechanism; A_{P} is the hyperfine coupling constant for the polarization mechanism; and $\vec{I}$ and $\vec{S}$ are the nuclear and electron spin operators, respectively.

The electron−nuclear dipolar interaction results in a broadening of the spectral lines and is expressed as

$$\hat{H}_{\text{DIP}}^{\text{paramagn}} = \frac{\mu_0}{4\pi}\bar{\mu}_{\text{e}}\tilde{D}_{\text{en}}\mu_{\text{n}} \quad (3)$$

where μ_0 is the magnetic permeability, $\bar{\mu}_{\text{e}}$ is the thermally averaged electronic magnetic moment, $\tilde{D}_{\text{en}}$ is the electron−nuclear dipolar coupling tensor, and μ_{n} is the nuclear magnetic moment. In the calculations, we employed the effective magnetic moment $\mu_{\text{eff}} = 3.13\ \mu_{\text{B}}$ (Bohr magneton) determined experimentally for the europium-substituted Keggin compounds.[22]

The electron−nuclear dipolar coupling tensor $\tilde{D}_{\text{en}}$ is expressed in a matrix representation:[24]

$$\tilde{D}_{\text{en}} = \frac{1}{r^3}(\delta_{\alpha\beta} - 3e_{\alpha}e_{\beta}) \quad (4)$$

where r is the electron−nuclear distance, $\delta_{\alpha\beta}$ is the Kronecker delta, and e_{α} and e_{β} are the (x, y, z) components of the electron−nuclear dipolar vector.

In the rare-earth-substituted polyoxoanionic solids under investigation, the electron−nuclear dipolar coupling matrices arising from the interactions of ^{31}P with multiple rare-earth sites have to be considered. It has been shown previously[23,24] that to a good approximation the local fields on the nucleus are independent contributions of the individual electrons. Thus, the total electron−nuclear dipolar Hamiltonian can be obtained by summing up the dipolar matrices corresponding to the individual electron−nuclear spin pairs:

$$\hat{H}_{\text{DIP}}^{\text{paramagn}} = \frac{\mu_0}{4\pi}\bar{\mu}_{\text{e}}\left(\sum_i \tilde{D}_{\text{en},i}\right)\mu_{\text{n}} \quad (5)$$

The summed dipolar coupling tensor is transformed to its principal axes system by diagonalization of the corresponding matrix, to obtain its eigenvalues δ_{xx}, δ_{yy}, and δ_{zz}, where by convention $|\delta_{zz} - \delta_{\text{iso}}| \geq |\delta_{xx} - \delta_{\text{iso}}| \geq |\delta_{yy} - \delta_{\text{iso}}|$. The principal components are subsequently defined as

$$\Delta\delta = \delta_{zz} - \frac{1}{2}(\delta_{xx} + \delta_{yy}) \quad (6)$$

$$\eta = \frac{\delta_{yy} - \delta_{xx}}{\delta_{zz} - \delta_{\text{iso}}} \quad (7)$$

$$\delta_{\text{iso}} = \frac{1}{3}(\delta_{xx} + \delta_{yy} + \delta_{zz}) \quad (8)$$

δ_{iso} is the isotropic shift; $\Delta\delta$ is the electron−nuclear dipolar anisotropy determining the breadth of the dipolar coupling tensor. η is the asymmetry parameters of the dipolar coupling tensor characterizing the deviation of the dipolar tensor from the axial symmetry.

It is worth noting that, for ^{31}P nuclei with relatively weak couplings to the paramagnetic center(s), the contribution of the ^{31}P CSA cannot be neglected. In this case, the effective anisotropy is a sum of the electron−nuclear dipolar and the CSA tensors. The experimental measurements will yield this combined interaction rather than the electron−nuclear dipolar anisotropy alone.

Results and Discussion

^{31}P MAS NMR Spectra and Isotropic Chemical Shifts of Diamagnetic Vanadium-Substituted and Paramagnetic Europium-Substituted Wells−Dawson Polyoxometalate Solids. The ^{31}P MAS NMR spectra are compared in Figure 2 for seven Wells−Dawson solids. Three of these solids are diamagnetic, substituted with V^{V}: cap-substituted 1-$K_7P_2VW_{17}O_{62}\cdot 18H_2O$ (**I**, α_2 isomer), belt-substituted 4-$K_7P_2VW_{17}O_{62}\cdot 17H_2O$ (**II**, α_1 isomer), and cap-substituted 1,2-$K_8P_2V_2W_{16}O_{62}\cdot 18H_2O$ (**III**). Four of the compounds are paramagnetic, containing Eu^{III} in the anion core, and include two α_2 isomers, the monomeric $Al_2(H_3O)_8[Eu(H_2O)_3(\alpha_2\text{-}P_2W_{17}O_{61})]_2\cdot 29H_2O$ (**IV**) and the dimeric $K_{17}[Eu(\alpha_2\text{-}P_2W_{17}O_{61})_2]$ (**V**), as well as two α_1 compounds, the monomeric $K_7[Eu(H_2O)_4(\alpha_1\text{-}P_2W_{17}O_{61})]$ (**VI**) and the dimeric $K_{14}(H_3O)_3[Eu(\alpha_1\text{-}P_2W_{17}O_{61})_2]\cdot 4KCl\cdot 64H_2O$ (**VII**) (the molecular structures depicted in Figure 1). The ^{31}P NMR spectra were acquired at the MAS frequency of 3 kHz for vanadium-substituted solids and at the MAS frequency of 10 kHz for europium-substituted solids. All spectra exhibit two sets of spinning-sideband manifolds, representing two individual phosphorus atoms in the Wells−Dawson anion. The spinning-sideband manifolds in the ^{31}P NMR spectra of the mono- and divanadium-substituted solids **I**−**III** span a very small range (ca. 60 ppm) compared with those for the europium-substituted solids (ca. 400 ppm), reflecting small CSAs in diamagnetic compounds. Furthermore, the two phosphorus sites in the diamagnetic compounds show similar spinning-sideband patterns and breadths of the spectral envelopes, indicating that the two central phosphorus atoms have similar CSAs. The isotropic ^{31}P solution shifts of the diamagnetic vanadium-substituted compounds **I**−**III** are given in Table 1 and are in excellent agreement with those reported previously.[32] The ^{31}P solid-state isotropic shifts of these diamagnetic compounds differ from the solution shifts (Table 1) and were assigned based on the direct ^{31}P−^{51}V interatomic distance measurements via REAPDOR spectroscopy.[44]

The broad spinning-sideband manifolds in the ^{31}P MAS NMR spectra of europium-substituted Wells−Dawson compounds (ca. 400 ppm) are attributed to the dominant electron−nuclear dipolar interaction, similar to what we

(44) Huang, W. Ph.D. Thesis, University of Delaware, Newark, DE, 2007.

Table 1. Experimental ^{31}P Solid-State and Solution NMR Parameters for the Vanadium- and Europium-Substituted Wells−Dawson Oxotungstates **I**−**VII**: ^{31}P Isotropic Chemical Shifts (δ_{iso}), Combined Electron−Nuclear Dipolar, and Chemical Shielding Anisotropies ($\Delta\delta$ and η)

		Solid-State NMR Parameters						Solution NMR Parameters	
		$\Delta\delta$,[b] ppm		η[b]		δ_{iso},[c] ppm ($\Delta\delta_{iso}$, ppm)		δ_{iso}, ppm for Experimental/Literature[32]	
Compounds		P1	P2	P1	P2	P1	P2	P1	P2
I[a]	1-$K_7P_2VW_{17}O_{62}\cdot 18H_2O$ (α_2 isomer)	28.4 ± 1.3	33.2 ± 0.8	0.10 ± 0.14	0.11 ± 0.16	10.4	8.3	−11.04/ −10.84	−13.11/ −12.92
II[a]	4-$K_7P_2VW_{17}O_{62}\cdot 17H_2O$ (α_1 isomer)	35.4 ± 4.1	32.7 ± 0.1	0.42 ± 0.40	0.21 ± 0.23	9.5	8.3	−11.64/ −11.83	−12.72/ −12.90
III[a]	1,2-$K_8P_2V_2W_{16}O_{62}\cdot 18H_2O$	25.2 ± 1.1	30.6 ± 0.1	0.01 ± 0.01	0.44 ± 0.14	12.5	7.6	−8.91/ −8.82	−13.23/ −13.44
IV	$Al_2(H_3O)_8[Eu(H_2O)_3(\alpha_2\text{-}P_2W_{17}O_{61})]_2\cdot 29H_2O$	179.6 ± 3.4	68.3 ± 2.6	0.34 ± 0.02	0.46 ± 0.15	27.7 (17.3)	9.6 (1.3)		
V	$K_{17}[Eu(\alpha_2\text{-}P_2W_{17}O_{61})_2]\cdot 42.5H_2O$	163.7 ± 11.2	55.8 ± 6.2[d]	0.25 ± 0.27	0.21 ± 0.21	22.9 (12.5)	7.2 (−0.9)		
VI	$K_7[Eu(H_2O)_4(\alpha_1\text{-}P_2W_{17}O_{61})]$	161.8 ± 3.5	77.9 ± 2.6	0.40 ± 0.06	0.25 ± 0.28	22.9 (13.4)	8.4 (0.1)		
VII	$K_{14}(H_3O)_3[Eu(\alpha_1\text{-}P_2W_{17}O_{61})_2]\cdot 4KCl\cdot 64H_2O$	124.9 ± 3.3	72.2 ± 9.8	0.52 ± 0.21	0.14 ± 0.17	18.3 (8.8)	8.7 (0.4)		

[a] For the diamagnetic Wells−Dawson solids **I**−**III**, δ and η are chemical shielding anisotropies. [b] These are values obtained by averaging the experimental parameters extracted from the spectra acquired at several different spinning frequencies. [c] Apparent paramagnetic shifts calculated as the difference between the observed chemical shift and the chemical shift for the corresponding vanadium analog. [d] For this site, the anisotropy was extracted using recycle delays of 10 and 60 s, due to the long T_1 (see Table 3). Within the experimental error indicated in Table 1, the derived anisotropies are the same.

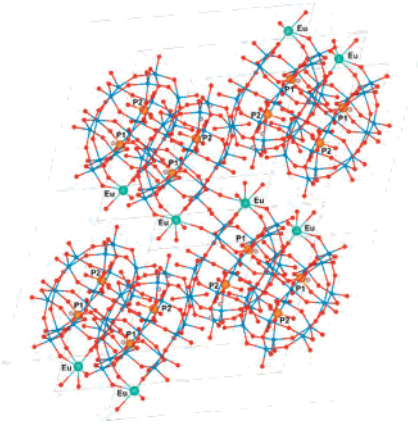

Figure 3. Coordination environment of the monomeric $Al_2(H_3O)_8[Eu(H_2O)_3(\alpha_2\text{-}P_2W_{17}O_{61})]_2\cdot 29H_2O$ (**IV**). The molecules are depicted in a ball-and-stick representation. In the anion, the tungsten atoms are shown in blue and the central phosphorus atoms are shown in orange. The europium atoms are shown in green.

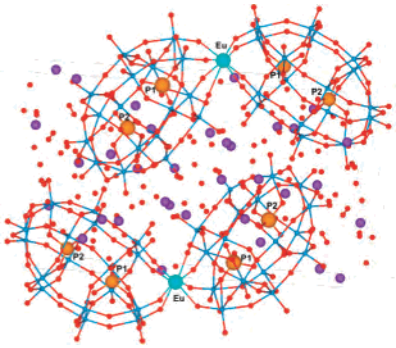

Figure 4. Coordination environment of the dimeric $K_{17}[Eu(\alpha_2\text{-}P_2W_{17}O_{61})_2]\cdot 42.5H_2O$ (**V**). The molecules are depicted in a ball-and-stick representation. In the anion, the tungsten atoms are shown in blue and the central phosphorus atoms are shown in orange. The europium atoms are shown in green.

observed previously in europium-substituted Keggin solids.[22] The two phosphorus atoms in the Wells−Dawson anion have distinct isotropic chemical shifts. The resonances can be readily assigned by inspection, based on the different breadths of the spinning-sideband manifolds associated with the two peaks reflecting the distance dependence of the electron−nuclear dipolar interaction (see eq 4). Based on the above, the broader spinning-sideband manifold is associated with the phosphorus site close to the paramagnetic Eu^{III} and arbitrarily designated as "P1" and the narrower spinning-sideband manifold with the more distant phosphorus site designated as "P2".

The isotropic chemical shifts of diamagnetic Wells−Dawson solids and effective isotropic shifts of paramagnetic Wells−Dawson solids are compiled in Table 1. As expected, the vanadium-substituted Wells−Dawson solids (**I**−**III**) exhibit small ^{31}P isotropic chemical shifts. Furthermore, these shifts are only slightly different for the two phosphorus sites. In contrast, the effective isotropic shifts in the paramagnetic compounds differ substantially for the two phosphorus atoms (see Table 1). The shift of the P1 site (the atom closer to the paramagnetic center) is significantly larger than that of P2, whereas the chemical shift of the P2 atom is quite similar to the shifts in the diamagnetic compounds. As discussed earlier, the observed isotropic shift in a paramagnetic solid is caused by the through-bond Fermi-contact shift and the much smaller through-space pseudocontact shift. The Fermi-contact shift is greatly reduced for larger numbers of bonds separating the atoms. The small differences in the isotropic shifts of P2 in paramagnetic versus diamagnetic solids indicate that the Fermi-contact interaction is weak for this site. This is expected because the Fermi-contact shift is generally negligible for a phosphorus atom (and generally any nucleus of interest) separated by more than four bonds from the paramagnetic center.[45]

The ^{31}P NMR spectra of vanadium- and europium-substituted Wells−Dawson solids **I**−**VII** at different spinning frequencies are shown in Figures 1S−7S of the Supporting

(45) Bertini, I.; Luchinat, C.; Parigi, G.; Pierattelli, R. *ChemBioChem* **2005**, *6*, 1536−1549.

Table 2. Calculated Electron−Nuclear Dipolar Interaction ($\Delta\delta$) for ^{31}P in Crystallographically Characterized Europium-Substituted Wells−Dawson Oxotungstates **IV**, **V**, and **VII**[a]

	100 Å		60 Å		35 Å		15 Å	
Compounds	$\Delta\delta$, ppm	η	$\Delta\delta$, ppm	η	$\Delta\delta$, ppm	η	$\Delta\delta$, ppm	η
IV	P1: 177.6	P1: 0.17	P1: 177.6	P1: 0.17	P1: 177.5	P1: 0.18	P1: 177.9	P1: 0.13
	P2: 39.3	P2: 0.16	P2: 39.4	P2: 0.15	P2: 37.9	P2: 0.16	P2: 41.5	P2: 0.17
V	P1: 167.7	P1: 0.01	P1: 167.6	P1: 0.01	P1: 167.4	P1: 0.02	P1: 166.1	P1: 0.02
	P2: 29.6	P2: 0.16	P2: 29.3	P2: 0.16	P2: 28.6	P2: 0.16	P2: 25.6	P2: 0.38
VII	P1: 146.6	P1: 0.04	P1: 146.4	P1: 0.04	P1: 146.1	P1: 0.04	P1: 145.2	P1: 0.04
	P2: 60.6	P2: 0.09	P2: 60.6	P2: 0.09	P2: 60.5	P2: 0.09	P2: 61.8	P2: 0.16

[a] Paramagnetic centers within 100, 60, 35, and 15 Å were included in the calculations.

Information. The electron−nuclear dipolar anisotropies for the two distinct phosphorus sites in the paramagnetic solids **IV**−**VII** were extracted by numerical analyses of the spinning-sideband intensities in these spectra as described previously,[22] and the results are reported in Table 1. The cap-substituted compounds **IV** and **V** (α_2 isomers) have different Eu^{III}/ligand ratios: 1:1 Eu/(α_2-$P_2W_{17}O_{61}$)$^{10-}$ and 1:2 Eu/(α_2-$P_2W_{17}O_{61}$)$^{10-}$, respectively. The anisotropies of the two phosphorus sites in **IV** are 179.6 ppm (P1) and 68.3 ppm (P2), while the corresponding parameters for **V** are 163.4 ppm (P1) and 55.8 ppm (P2). These pronounced differences in the anisotropies reflect the different local environments of europium sites in these two compounds. These results are in agreement with the X-ray structures of these compounds presented in Figures 3 (**IV**) and 4 (**V**). The X-ray structure of **IV** shows that the monomer is connected to form a 2:2 complex wherein a Eu−O from one (α_2-$P_2W_{17}O_{61}$)$^{10-}$ unit is connected to a belt W−O of the adjacent (α_2-$P_2W_{17}O_{61}$)$^{10-}$ unit. This structure renders the P1 and P2 sites closer to the second Eu^{III} than in compound **V**. According to the X-ray coordinates, the distances between P1 and the two closest europium atoms are 4.34 and 7.36 Å in **IV**, whereas the same distances are 4.43 and 10.72 Å in **V**. Similarly, the corresponding P2−Eu distances are 7.94 and 8.04 Å in **IV**, whereas the same distances are 8.06 and 13.13 Å in **V**. The more distant europium atoms in the crystal lattice are more than 13 Å away from the phosphorus atoms, and their contributions to the electron−nuclear dipolar coupling are relatively weak.

In the belt-substituted α_1 isomers **VI** [1:1 Eu/(α_1-$P_2W_{17}O_{62}$)$^{10-}$] and **VII** [1:2 Eu/(α_1-$P_2W_{17}O_{62}$)$^{10-}$], numerical analyses of the ^{31}P MAS NMR spectra yielded the following electron−nuclear dipolar anisotropies: 161.8 ppm (P1) and 77.5 ppm (P2) in **VI**; 124.9 ppm (P1) and 72.5 ppm (P2) in **VII**. These values indicate different local geometries of europium ions in these two α_1 species, similar to the cap-substituted α_2 isomers. The X-ray structure of **VII** indicates that the P1−Eu distances are 4.62 and 11.61 Å; the corresponding P2−Eu distances are 6.15 and 12.91 Å. There is no crystal structure of **VI**; however, on the basis of the larger electron−nuclear dipolar anisotropy and of the results for the cap-substituted isomers **IV** and **V**, we expect that the P1−Eu distances will be shorter than those in **VII**. The above results demonstrate that ^{31}P NMR spectra are a sensitive probe of the local geometry of paramagnetic europium centers in the Wells−Dawson solids and reveal subtle differences in the local environments even in homologous structures.

Calculations of the Electron−Nuclear Dipolar Coupling Tensors in Crystallographically Characterized Paramagnetic Europium-Substituted Wells−Dawson Solids. The electron−nuclear dipolar anisotropies were calculated for the two central phosphorus sites in the three paramagnetic Wells−Dawson solids **IV**, **V**, and **VII** using their known X-ray crystallographic structures and adopting the point-dipole approximation. The electron−nuclear dipolar matrices were calculated by first considering only those europium atoms within 15 Å to the phosphorus atom and then subsequently including additional europium sites that are within 35, 60, and 100 Å. The results of the calculations are shown in Table 2.

According to the results, the dominant contributions to the electron−nuclear dipolar interactions arise from the europium atoms that are within 15 Å to the phosphorus sites (more than 99% contribution to the P1 anisotropies and more than 90% to the P2). Therefore, the intramolecular europium and a europium atom in one of the adjacent molecules have the largest effect on the anisotropy. This is in contrast to Keggin solids, where several adjacent anions have to be taken into account in order to obtain an accurate prediction of the electron−nuclear dipolar anisotropies.[22] This result is not entirely surprising in light of the larger size of the Wells−Dawson oxotungstate anions and the larger unit cells.

For the two α_2 isomers (**VI** and **VII**), the calculated anisotropies $\Delta\delta$ of the P1 sites show very good agreement with the experimental results (see Tables 1 and 2 and Figure 5), while the calculated anisotropies $\Delta\delta$ for the P2 sites are consistently smaller than the experimental values. The discrepancies between the experimental and calculated anisotropies for the P2 site are 26−29 ppm; these values are very similar to the CSAs for the corresponding phosphorus sites in the diamagnetic vanadium-substituted Wells−Dawson solids (Table 1). Therefore, we conclude that the experimental effective anisotropies of the P2 sites contain contributions from the electron−nuclear dipolar interaction and from the chemical shielding interaction and that both terms are similar. This is not surprising because electron−nuclear dipolar interaction of the P2 site is relatively weak, and therefore the CSA term becomes of comparable magnitude. For the α_1 isomer (**VII**), the calculated anisotropy of P1 is larger by 20 ppm than that from experiments. This is not clearly understood. The most likely explanation is that

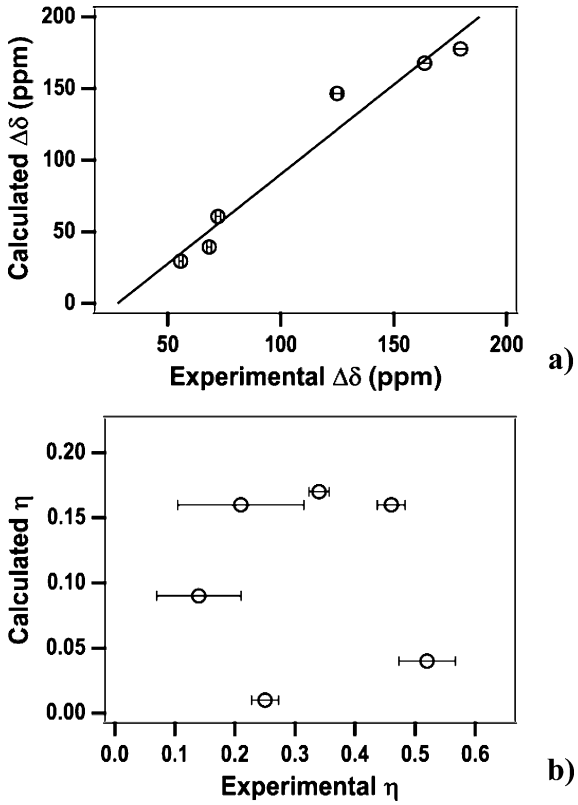

Figure 5. Comparison of experimental and calculated anisotropic NMR observables $\Delta\delta$ (a) and η (b) for crystallographically characterized compounds **IV**, **V**, and **VII**. For $\Delta\delta$, a linear correlation between the experimental and calculated parameters was observed: $\Delta\delta_{calc} = -34.8 + 1.25\Delta\delta_{exp}$. The NMR parameters were calculated by including the paramagnetic centers within 100 Å from the phosphorus nucleus.

Table 3. ^{31}P Spin−Lattice (T_1) and Spin−Spin (T_2) Relaxation Parameters of Wells−Dawson Solids at $T = 293$ K

	T_1 (s)		T_2 (ms)	
Compounds	P1	P2	P1	P2
I	3.3	33.1	55	53
II	1.5	5.7	71	81
III	6.5	29.1	76	82
IV	2.1	36.8	36	39
V	3.7	159.0	35	46
VI	5.3	36.1	33	58
VII	5.5	26.6	35	55

the effective magnetic moment of Eu^{III} in this compound is smaller than 3.13 μ_B, which is the effective magnetic moment experimentally determined for the europium-substituted Keggin solid $Li[Eu_2PW_{11}O_{34}]$.[22] We do not have the experimental value of the effective magnetic moment of **VII**, but in light of the variations in the magnetic moments observed in the Keggin solids observed in our earlier work,[22] this is a logical assumption.

The experimental and calculated asymmetry parameters are not in any agreement, with the experimental values being generally much higher than the predictions (illustrated in Figure 5b). We have observed similar behavior in the europium-substituted Keggin solids.[22] We attribute this to the generally low accuracy in the experimental values of the asymmetry parameters as a result of the conformational heterogeneity in the sample, so that the spinning-sideband intensities cannot be defined accurately.

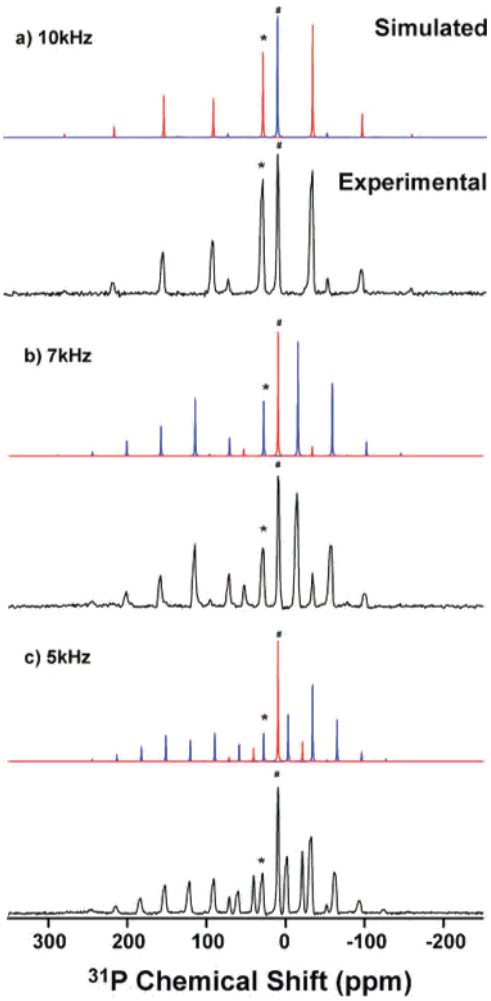

Figure 6. Bottom: ^{31}P MAS NMR spectra of $Al_2(H_3O)_8[Eu(H_2O)_3(\alpha_2\text{-}P_2W_{17}O_{61})]_2\cdot 29H_2O$ (**IV**). Top: ^{31}P NMR spectra of **IV** calculated using the values given in Table 2 at different spinning frequencies: (a) 10 kHz; (b) 7 kHz; (c) 5 kHz. The isotropic bands for the two crystallographically distinct phosphorus atoms are indicated with an asterisk (P1) and a pound (P2). The observed isotropic shifts of the calculated spectra are taken from those of the corresponding phosphorus atom in the experimental spectra for consistency.

To illustrate the above Results and Discussion, the spectra simulated using the NMR parameters ($\Delta\delta$ and η) calculated from the X-ray coordinates (Table 2) are plotted in Figures 6−8 for $Al_2(H_3O)_8[Eu(H_2O)_3(\alpha_2\text{-}P_2W_{17}O_{62})]_2\cdot 29H_2O$ (**IV**), $K_{16}(H_3O)[Eu(\alpha_2\text{-}P_2W_{17}O_{61})_2]\cdot 42.5H_2O$ (**V**), and $K_{14}(H_3O)_3[Eu(\alpha_1\text{-}P_2W_{17}O_{62})_2]\cdot 4KCl\cdot 64H_2O$ (**VII**), respectively, together with the corresponding experimental spectra acquired at different spinning frequencies.

^{31}P Spin−Lattice and Spin−Spin Relaxation Times in Vanadium- and Europium-Substituted Wells−Dawson Solids. The spin−lattice and spin−spin relaxation times (T_1 and T_2) for the two phosphorus sites (P1 and P2) in diamagnetic and paramagnetic Wells−Dawson solids are summarized in Table 3. Interestingly, the spin−lattice relaxation times (T_1) of the two phosphorus atoms in both vanadium and europium Wells−Dawson oxotungstate anions are different from each other. As expected, P1 (which is closer to the quadrupolar nucleus or paramagnetic ion) has a shorter T_1 than P2. The relaxation mechanisms of phos-

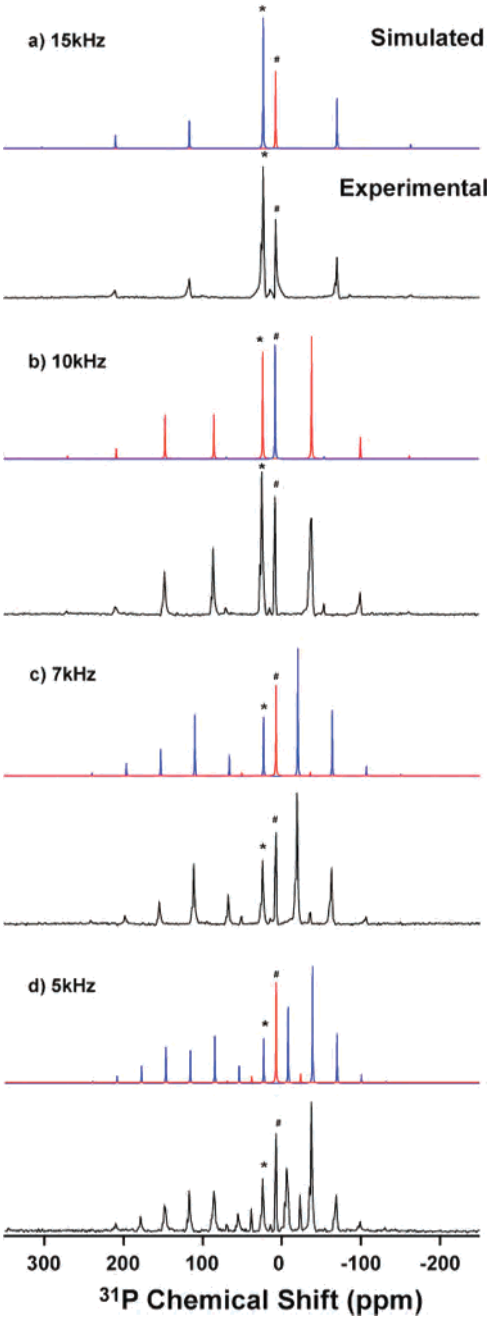

Figure 7. Bottom: ^{31}P MAS NMR spectra of $K_{17}[Eu(\alpha_2\text{-}P_2W_{17}O_{61})_2]\cdot 42.5H_2O$ (**V**). Top: ^{31}P NMR spectra of **V** calculated using the values given in Table 2 at different spinning frequencies: (a) 15 kHz; (b) 10 kHz; (c) 7 kHz; (d) 5 kHz. The isotropic bands for the two crystallographically distinct phosphorus atoms are indicated with an asterisk (P1) and a pound (P2). The observed isotropic shifts of the calculated spectra are taken from those of the corresponding phosphorus atom in the experimental spectra for consistency.

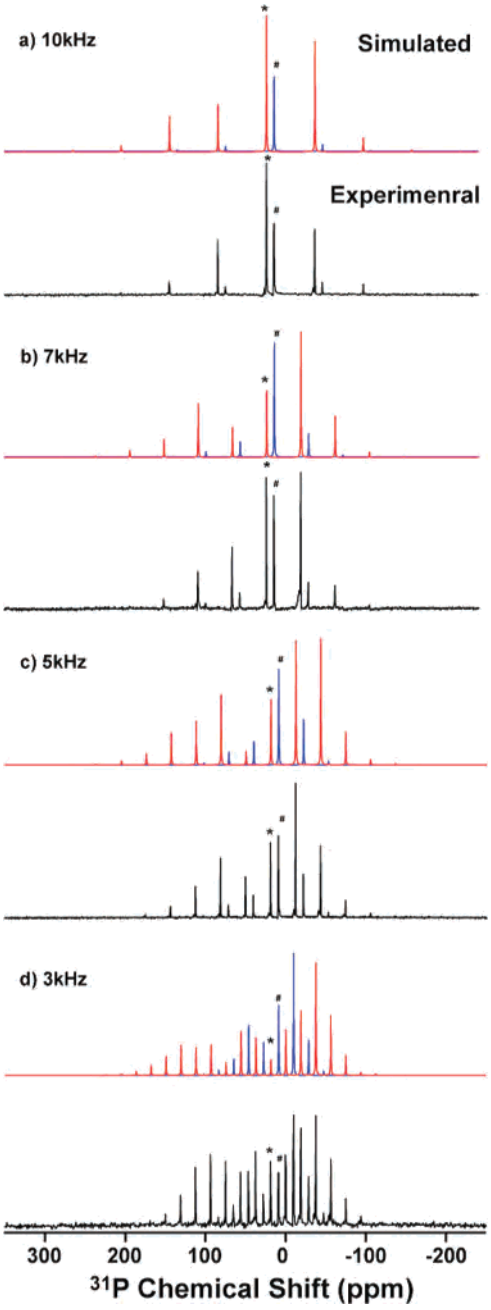

Figure 8. Bottom: ^{31}P MAS NMR spectra of $K_{14}(H_3O)_3[Eu(\alpha_1\text{-}P_2W_{17}O_{61})_2]\cdot 4KCl\cdot 64H_2O$ (**VII**). Top: ^{31}P NMR spectra of **VII** calculated using the values given in Table 2 at different spinning frequencies: (a) 10 kHz; (b) 7 kHz; (c) 5 kHz; (d) 3 kHz. The isotropic bands for the two crystallographically distinct phosphorus atoms are indicated with an asterisk (P1) and a pound (P2). The observed isotropic shifts of the calculated spectra are taken from those of the corresponding phosphorus atom in the experimental spectra for consistency.

phorus nuclei in vanadium-substituted diamagnetic and europium-substituted paramagnetic Wells−Dawson solids are different. Both quadrupolar and paramagnetic interactions give rise to efficient relaxation mechanisms, and in both cases, the proximity of the phosphorus atom to the quadrupolar (^{51}V) or paramagnetic (Eu^{III}) site results in short relaxation times. The spin−lattice relaxation time T_1 depends on the electron−nuclear dipolar coupling and is proportional to the inverse of the sixth power of the paramagnetic center-to-nucleus distance.[46] The shorter T_1 in P1 in paramagnetic solids reflects a stronger coupling between ^{31}P and the europium ion and short P1−Eu distances. In diamagnetic compounds, the ^{31}P spin−lattice relaxation induced by the quadrupolar interaction with the ^{51}V site depends on the ^{31}P−^{51}V distance as well.

(46) Bertini, I.; Luchinat, C. *NMR of Paramagnetic Molecules in Biological Systems*; The Benjamin/Cummings Publishing Co., Inc.: Menlo Park, 1986.

The spin−spin relaxation times (T_2) of the two central phosphorus atoms exhibit only slight differences, and P1 has a shorter T_2 time than P2 in all of the Wells−Dawson solids except **I**, where the relaxation times for the two sites are very similar.

This relaxation study indicates that the spin−lattice relaxation times are sensitive to the local geometry of europium and vanadium ions surrounding the ^{31}P nucleus in Wells−Dawson solids, but the relaxation rates alone are not sufficient for deriving any structural information.

Conclusions

Anisotropic electron−nuclear dipolar interaction dominates the ^{31}P MAS NMR spectra of europium-substituted polyoxoanionic solids of the Wells−Dawson family. The local arrangements of the paramagnetic centers with respect to the phosphorus sites are dictated by positional isomerism and by the anion stoichiometry and, in turn, have a significant impact on the magnitude and the asymmetry parameter of the electron−nuclear dipolar tensor. The electron−nuclear dipolar anisotropies extracted from the experimental spectra and those calculated from the X-ray coordinates are in good agreement, suggesting that ^{31}P MAS NMR spectroscopy can be a quick and useful probe of paramagnetic environments in this class of compounds.

Acknowledgment. The authors thank Dr. Cheng Zhang and Dr. Robertha Howell for the synthesis of europium-substituted Wells−Dawson compounds used in this study. T.P. acknowledges the financial support of the National Science Foundation (NSF-CAREER CHE-0237612) and the National Institutes of Health (Grant P20-17716, COBRE individual subproject). L.C.F. acknowledges the financial support of the National Science Foundation (NSF Grant CHE 0414218) and of the National Institutes of Health (Grant NIH-S06 GM60654 (SCORE)) and NSF Grant MRI0116244 for the purchase of an X-ray diffractometer. Research infrastructure at Hunter College is partially supported by NIH-Research Centers in Minority Institutions Grant RR03037-08.

Supporting Information Available: ^{31}P MAS NMR spectra of **I**−**VII** (Figures 1S−7S). This material is available free of charge via the Internet at http://pubs.acs.org.

IC700521P